ACS MATERIALS Au
AN OPEN ACCESS JOURNAL OF THE AMERICAN CHEMICAL SOCIETY

pubs.acs.org/materialsau

Article

Selective Conversion of CO_2 into Cyclic Carbonate on Atom Level Catalysts

Zhiqiang Zheng, Zhongqiang Wang, Yurui Xue,* Feng He,* and Yuliang Li*

Cite This: *ACS Mater. Au* 2021, 1, 107−115

Read Online

ACCESS | Metrics & More | Article Recommendations | Supporting Information

ABSTRACT: The conversion of carbon dioxide (CO_2) into organic carbonates under ambient temperatures and pressures with high conversion and selectivity still faces a great challenge. The zerovalent atomic catalysts (ACs), featuring accurate structure and valence states, provide a new and accurate model system for catalysis. Herein we developed a general preadsorption-reduction strategy to synthesize zerovalent cobalt AC on graphdiyne (Co^0/GDY). The Co^0/GDY ACs were used for efficient and selective CO_2 fixation. We were surprised to find that Co^0/GDY ACs reached nearly 100% conversion at 80 °C and 1 atm in CO_2 fixation and with a significantly high turnover frequency (TOF) of 3024.8 h^{-1}, which is almost several orders larger than that of benchmarked catalysts. Such high conversion and selectivity represent the advantages of emerging catalysts.

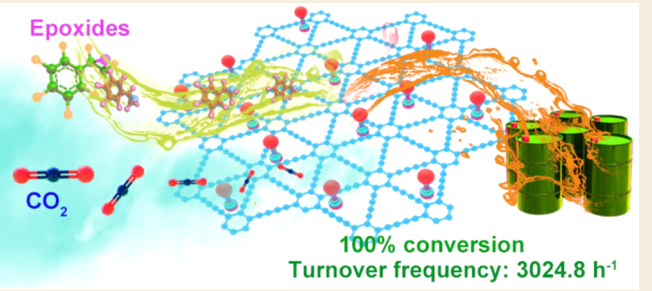

KEYWORDS: *Graphdiyne, two-dimensional carbon material, atomic catalysis, CO_2 fixation*

INTRODUCTION

Infinite carbon dioxide (CO_2) emission and nondegradable plastic pollution seriously hinder the sustainable development of energy and environment.[1−7] Reducing carbon emissions has become the common responsibility of the international community, so it is of great scientific significance to explore the efficient transformation of carbon dioxide. A potentially successful route is the efficient cycloaddition of CO_2, and epoxide into cyclic carbonate (the monomer for degradable aliphatic polycarbonate) provides an attractive route to address these challenges.[8] Over the past many years, countries around the world have devoted considerable financial, material, and human resources to the development of efficient catalysts, and the related results, particularly in industrialization, remain unsatisfactory.[9−14] For instance, as a pioneering work, homogeneous catalysts (e.g., Schiff or ionic liquids-based catalysts and metal complexes)[15−17] demonstrate high selectivity but face difficulties in product separation and recycling. Although heterogeneous catalysts are easy to separate from the reaction mixture, the reported catalysts such as metal−organic frameworks usually showed harsh synthesis conditions and low yield and catalytic activity.[18−24] The current situation is that neither homogeneous nor heterogeneous catalysts have absolute advantages in catalytic reactions. Therefore, in view of the current important position of catalysts in industry, the development and exploration of new types of catalysts can effectively activate reactions under ambient conditions with high selectivity, activity, and durability.[25]

Atomic catalysts (ACs), monodisperse metal atoms as active sites during the catalysis process, are considered to have 100% metal atom utilization and unique advantages to achieve high catalytic selectivity, activity, and stability in numerous reactions.[26−32] With the rapid development of ACs, some important scientific issues have attracted people's attention: (i) the precise selection of support materials; (ii) the characterization and exact structure of metal atoms anchored on support; (iii) the controllable changes of valence and configuration of metal atoms and the stability of atomic anchoring. These key issues are seen as important challenges in this field. Clear understanding of these key issues plays an important role in advancing traditional single-atom catalysts (TSACs) in structure, mechanism and determination of catalytic active sites. After solving these issues, it is possible to promote the great development of catalytic industry and create value for society at a high speed.

Graphdiyne (GDY), a new two-dimensional carbon allotrope with hexagonal benzene (sp^2-C) rings linked by diacetylenic (sp-C) bonds, has been proven to be a completely novel model platform to the catalysis and energy conversion system.[29−42] The rich acetylenic bonds (−C≡C−) endow

Received: April 19, 2021
Published: August 7, 2021

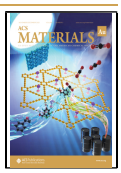

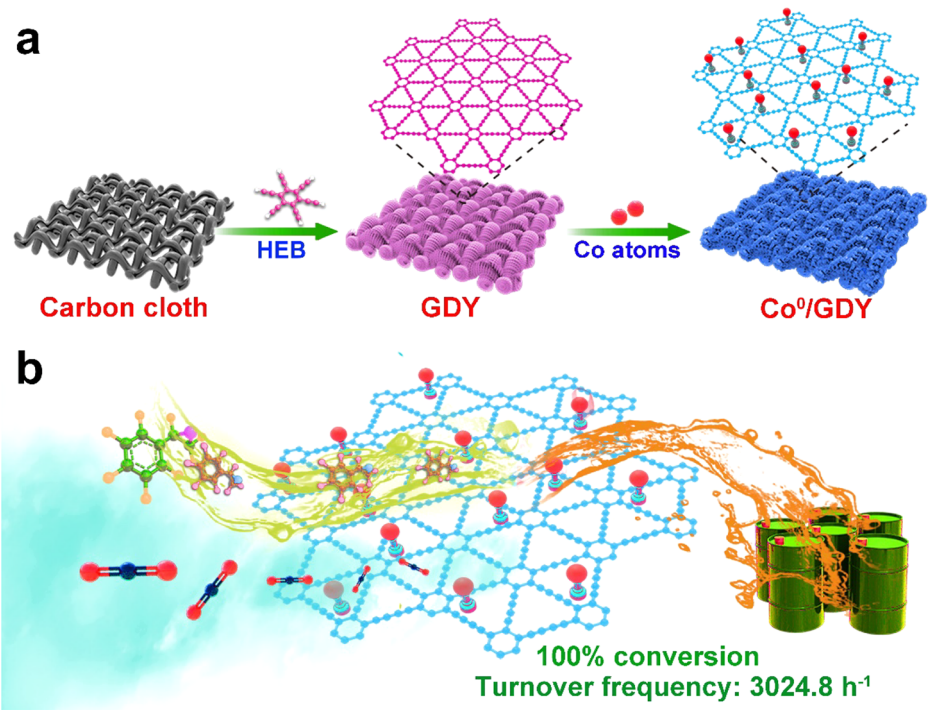

Figure 1. Schematic representation of (a) synthesis of Co^0/GDY and (b) corresponding selective conversion of CO_2 into cyclic carbonates.

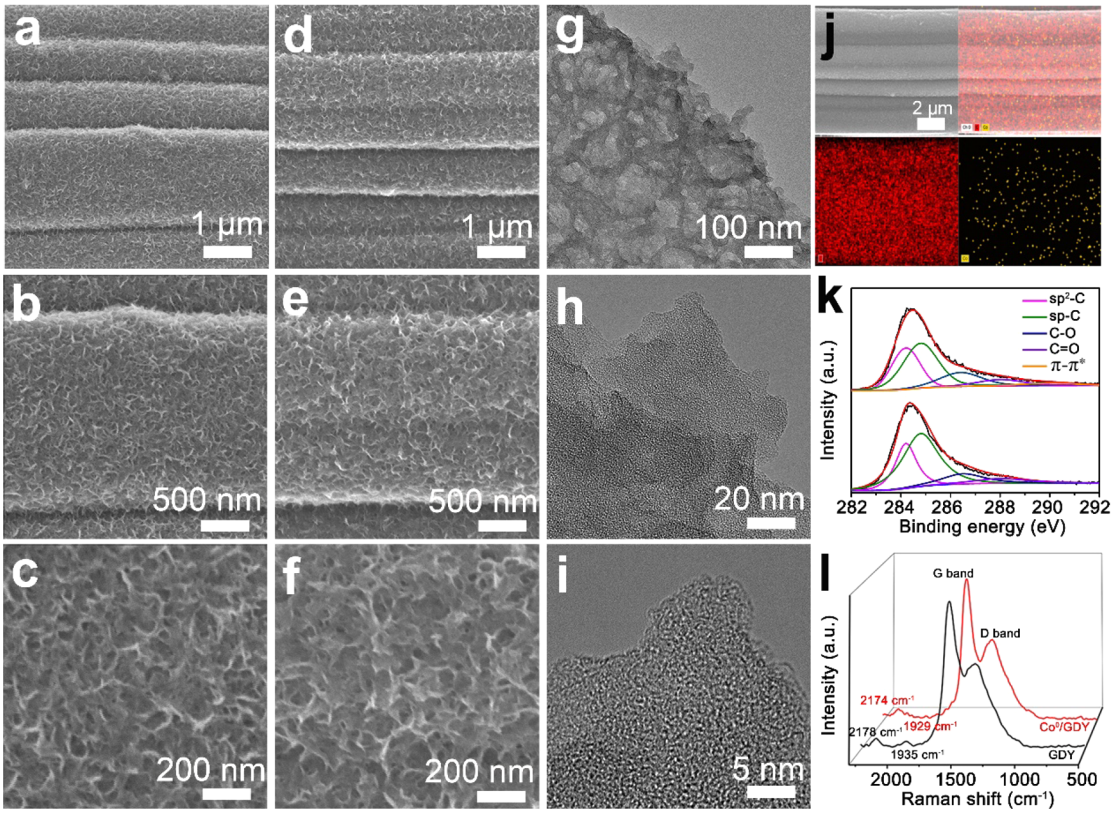

Figure 2. Low- and high-magnification SEM images of (a–c) pure GDY and (d–f) Co^0/GDY electrodes. (g) TEM and (h, i) HRTEM images of Co^0/GDY nanosheets. (j) Corresponding element mapping images of C and Co. (k) C 1s XPS spectra and (l) Raman spectra of Co^0/GDY and GDY.

GDY with many unique properties including the highly uneven distributed surface charge, natural pores, large surface area, unique abundant conjugated electronic structures, higher conductivity, and high stability.[43−47] Especially, the sp-hybridized −C≡C− in GDY allows for the arbitrary angle rotation of π/π^* perpendicular to the axis, therefore possibly pointing toward surrounding metal atoms, which make the easy chelation of metal atoms.[29,37,48] GDY has also been

https://doi.org/10.1021/acsmaterialsau.1c00012
ACS Mater. Au 2021, 1, 107−115

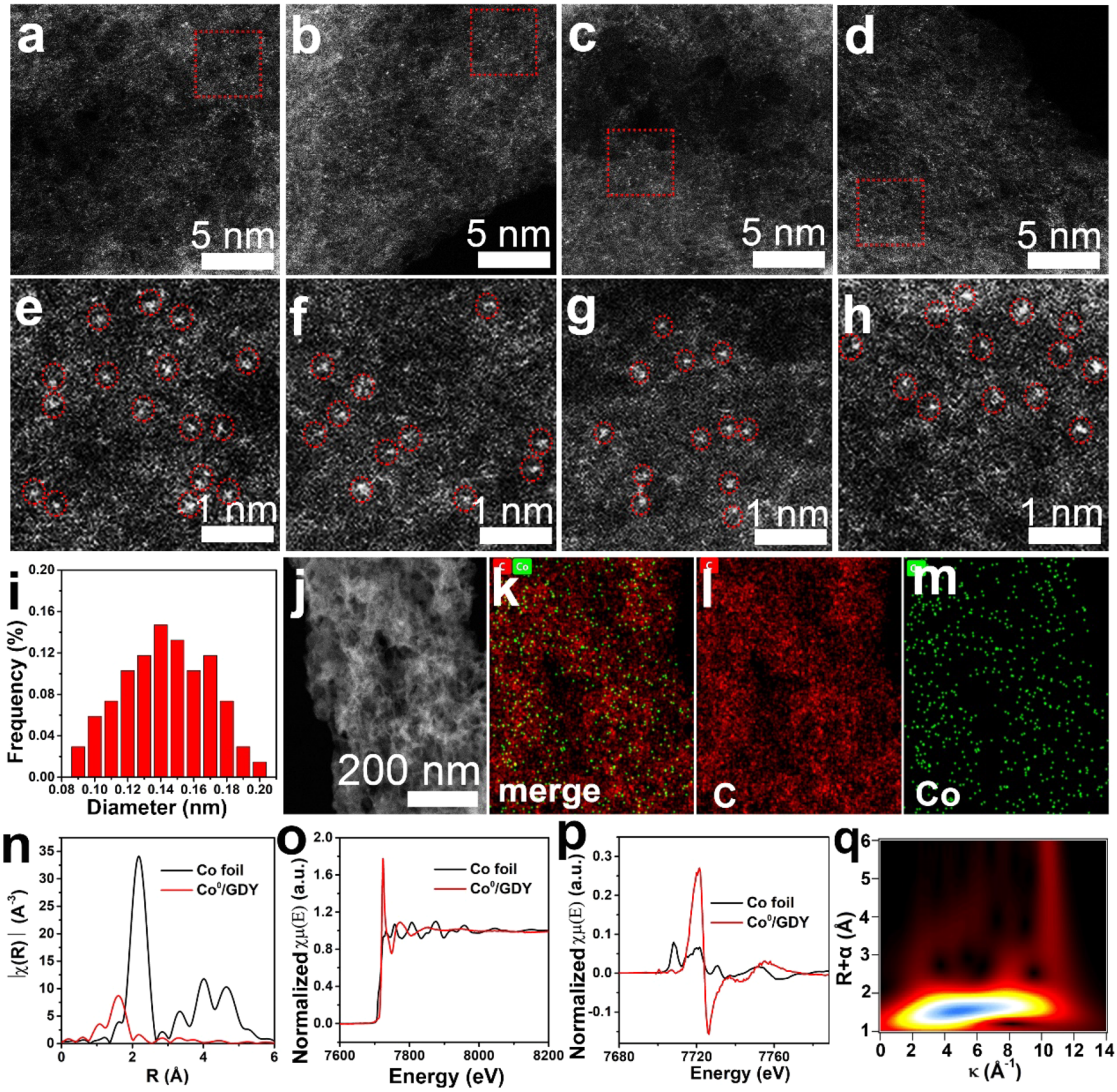

Figure 3. HAADF-STEM images of as-prepared Co^0/GDY: (a−d) four different regions; (e−h) corresponding enlargement of the marked regions in (a)−(d). Metal atoms are indicated by red circles. (i) STEM and (j) overlapping images and corresponding elemental mapping of (k) C and (l) Co in Co^0/GDY. (m) Size distribution of metal atoms counted from HAADF-STEM images. (n) EXAFS spectra of Co^0/GDY and Co foil. (o) Normalized Co Kedge XANES spectra of Co^0/GDY and Co foil (inset: first derivative curves). (p) Wavelet transforms for the k^3-weighted EXAFS signals of Co^0/GDY with optimum resolutions at 2.0 Å.

demonstrated to be the first carbon material that can anchor metal atoms without any additional treatments, which provides an excellent opportunity to fabricate stable ACs through a fast, efficient, and scalable way. Moreover, the definite chemical structure of GDY allows for the identification of the accurate structure of active sites, exploration of reaction process, and complete understanding of the mechanisms of the catalytic process. Owing to these advantages, accurate anchoring and high dispersion of the zerovalent metal atoms have been achieved by Li and co-workers,[29,38] resolving the bottleneck of the easy migration, aggregation, and charge transfer instabilities of TSACs on supports. Their results also revealed that the excellent catalytic activities of ACs originate from the incomplete charge transfer between the metal atoms and GDY. The unique structure and properties together with the excellent catalytic performances of ACs make them great potential candidates for next-generation catalysts. Moreover, the electrochemical deposition method, a process where the metallic ion can be easily reduced and anchored on the cathode surface, has been demonstrated to be a universal route for fabricating various atomic catalysts.[37,49]

Here, we systematically investigated the preparation, characterization, structure and properties of GDY-based zerovalent cobalt metal ACs (Co^0/GDY). The catalyst demonstrated excellent comprehensive performance for efficient CO_2 fixation under mild conditions. High-angle annular dark field scanning transmission electron microscopy (HAADF-STEM) imaging and X-ray absorption near-edge structure (XANES) results clearly showed all metal atoms are independently anchored on the surface of GDY. The unique interactions and charge transfer behavior between Co atoms and GDY greatly increase the amounts of active sites, endowing the ACs with superior catalytic performance, showing high conversion (near 100%) and selectivity (>99%) within 10 h of reaction. Very interestingly, Co^0/GDY exhibits the highest conversion of 100% with selectivity > 99% at low temperatures (80 °C) and the largest TOF value of

https://doi.org/10.1021/acsmaterialsau.1c00012
ACS Mater. Au 2021, 1, 107−115

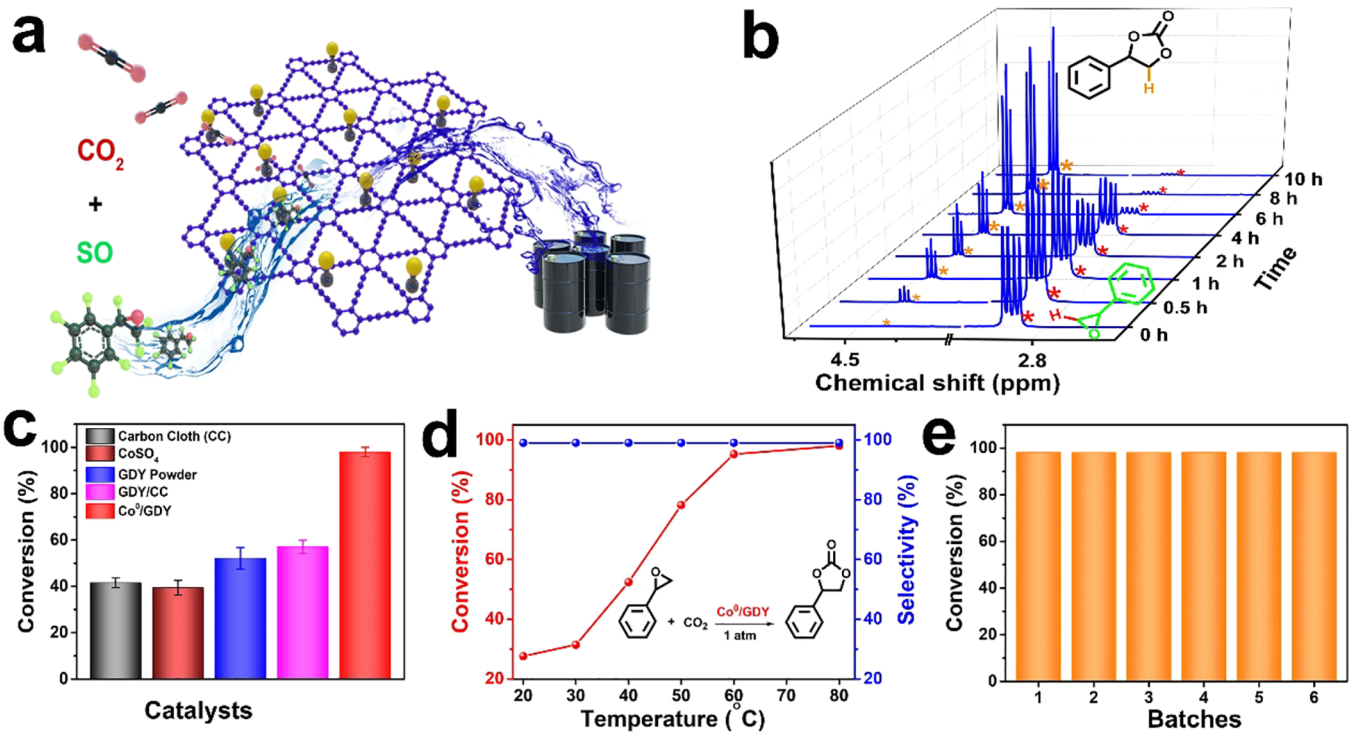

Figure 4. (a) Schematic representation of the CO_2−SO cycloaddition reaction. (b) Time course of the ^1H NMR results of the catalytic product by Co^0/GDY (bottom). (c) Catalytic performance of the Co salt, carbon cloth (CC), pure GDY powder, and GDY/CC for the CO_2−SO cycloaddition reaction at 80 °C. (d) Temperature course of the conversion and selectivity catalyzed by Co^0/GDY. (e) Six independent experiments for fresh-prepared Co^0/GDY.

3024.8 h^{-1}, which is almost several orders larger than benchmarked catalysts.

RESULTS AND DISCUSSION

Synthesis and Structural Characterizations

The facile preadsorption-reduction strategy was employed for the fabrication of Co^0/GDY (Figure 1), including the in situ growth of GDY, adsorption of metal ions, and in situ anchoring of metal atoms. It was observed from the scanning electron microscopy (SEM) images that a film of vertically aligned GDY nanosheets was directly grown on the smooth surface of the carbon cloth (Figures 2a−c and S1), forming a three-dimensional (3D) network with porous structure. Subsequently, the obtained 3D GDY electrode was immersed in a 0.5 M sulfuric acid solution containing 5 mM Co ions. The Co^0/GDY catalysts were obtained after an easy reduction treatment. This mild process is nondestructive, and the as-prepared Co^0/GDY retains the same morphology to that of pristine GDY (Figure 2d−f). Further, high-resolution transmission electron microscopy (TEM) analysis revealed that no nanodots or clusters can be observed on the Co^0/GDY nanosheets (Figure 2g−i), indicating the atomic dispersion of the anchored metal species on GDY. Elemental analysis of Co^0/GDY revealed the uniform dispersion of the Co atoms on GDY nanosheets (Figure 2j). As shown in Figure 2k, the C 1s XPS spectrum of Co^0/GDY shows five peaks at 284.2 eV for sp^2-C, 284.8 eV for sp-C, 286.5 eV for C−O, 288.0 eV for C═O, and 290.0 eV for the $\pi-\pi^*$ transition. Compared with the case of pristine GDY, the newly appeared $\pi-\pi^*$ transition peaks should be due to the synergetic interactions between metal species and GDY. XPS analysis also proved that there was no aggregated state of metal present (Figure S2). The 1:2 ratio of sp^2 to sp carbon atoms from the C 1s X-ray photoelectron spectroscopy (XPS) spectrum (Figures 2k and S2) and the peak at around 2178 cm^{-1} corresponding to the C≡C vibration in Raman spectra (Figure 2l) confirm the integrity of GDY after the anchoring of metal atoms. In addition, the Raman spectra showed no peaks at a low wavenumber (Figure S3a, 45−500 cm^{-1}), revealing that there are no metal-related peaks in the Co^0/GDY sample. Compared with original GDY, Co^0/GDY shows a slight shift in the diffraction peaks of diyne groups, indicating the interactions between Co atoms and acetylenic bonds. Co^0/GDY has a larger D/G ratio than that of pristine GDY (Figure 2l and S3b), revealing the formation of more defects that benefit to the generation of more active sites, therefore enhancing the catalytic efficiency. The metal loading was determined using inductively coupled plasma mass spectrometry (ICP-MS, Table S1).

HAADF-STEM was employed to characterize the morphology of the catalyst. In HAADF-STEM images (Figure 3a−h) each stands for a metal atom. Figure 3a−h clearly shows the isolated individual Co atoms were uniformly anchored on the surface of GDY. The average sizes of the Co atoms were measured to be 1.40 ± 0.06 nm (Figure 3i), with a narrow size distribution. Elemental mapping results further confirmed the uniform distribution of the Co atom on GDY (Figures 3j−m). From the X-ray adsorption fine structure (EXAFS) results, only one notable peak at 1.60 Å corresponding to Co−C, which is shorter than the Co−Co peak (2.17 Å), could be observed, indicating there are no corresponding Co−Co interactions and the isolated Co atoms anchored on GDY (Figure 3n). The XANES spectra of Co^0/GDY and Co foils (Figure 3o) indicate the zero-valence states of the Co atoms in as-prepared ACs, which is further determined by comparison

https://doi.org/10.1021/acsmaterialsau.1c00012
ACS Mater. Au 2021, 1, 107−115

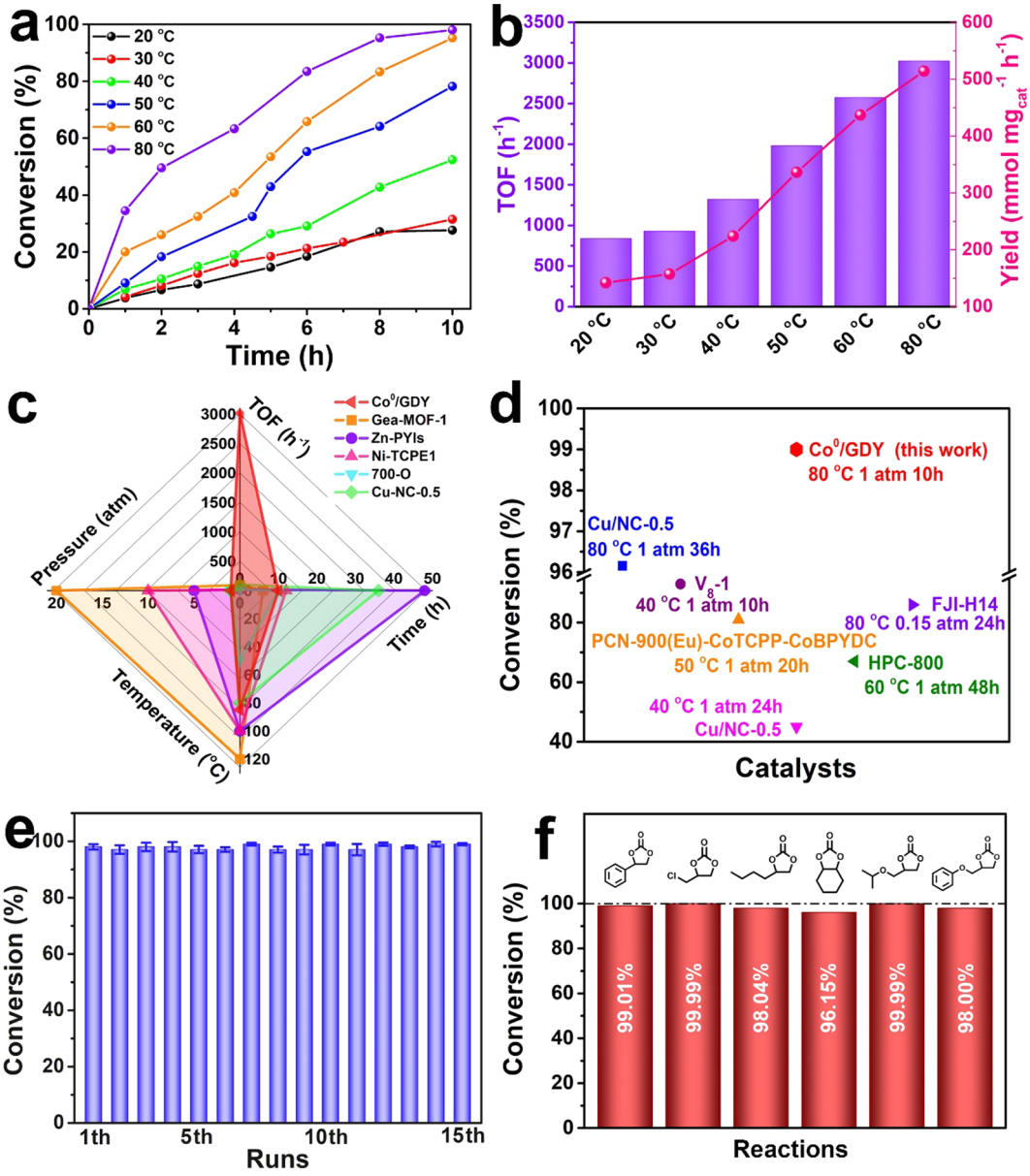

Figure 5. (a) Time course of catalytic conversion at different temperatures. (b) TOF value and product yields of Co^0/GDY at different temperatures. Comparison of (c) the TOF value and (d) the SO conversion of Co^0/GDY with reported catalysts. (e) Stability test of the catalyst. (f) Different substituent carbonates from corresponding epoxides catalyzed by Co^0/GDY under the same conditions.

of the first derivative spectra of Co^0/GDY with Co foils (Figure 3p). The wavelet transform (WT) analysis was performed to further confirm the dispersion state of Co species in Co^0/GDY (Figure 3q). It can offer more powerful resolution in both R and k spaces, and the intensity maximum ascribed to the coordination of Co is not observed at approximately 6.8 $Å^{-1}$. The highly dispersed Co atoms offer highly dispersed active sites for catalysis. Moreover, according to our previous studies, the zerovalent ACs possessed unique incomplete charge transfer behavior, beneficial for enhancing the catalytic activity. Benefiting from the above-mentioned fascinating properties, the as-prepared Co^0/GDY are supposed to have excellent catalytic performances.

Catalytic Performance Measurements

CO_2−epoxide cycloaddition reaction was selected as the probing reaction for evaluating the catalytic performance of Co^0/GDY under mild conditions in a solvent-free environment (Figure 4a). ^1H NMR spectroscopy was used to monitor the extent of the cycloaddition reaction (Figures 4b and S5−S16). It was observed from Figure 4b that no carbonate could be detected before the reaction was started. With the progression of the reaction, the characteristic peaks corresponding to the carbonates (orange star) appeared and gradually increased. Simultaneously, the peaks corresponding to styrene oxide (SO, red star) became smaller and smaller until they disappeared. Figure 4c showed that the corresponding Co salt, carbon cloth (CC), pure GDY powder, and GDY/CC had much lower catalytic performances below half of that obtained with the Co^0/GDY catalyst for the CO_2−SO cycloaddition reaction at 80 °C. These results revealed the excellent catalytic performance of GDY-based zerovalent Co atomic catalysts for the CO_2−SO cycloaddition reaction. Moreover, the cycloaddition reaction of SO with CO_2 for Co^0/GDY exhibited a small SO conversion of 1% without the presence of tetrabutylammonium

https://doi.org/10.1021/acsmaterialsau.1c00012
ACS Mater. Au 2021, 1, 107−115

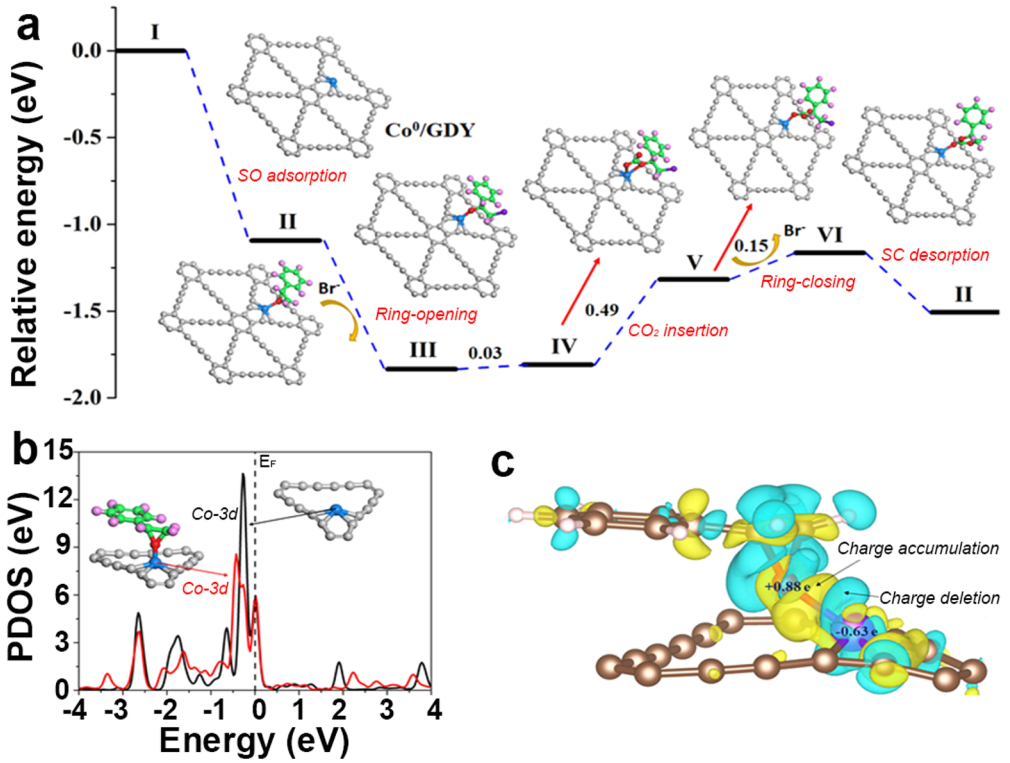

Figure 6. (a) DFT-calculated free energy profiles with the involved key intermediates after geometry optimizations for the cycloaddition of styrene oxide (SO) and CO_2 catalyzed by Co^0/GDY. Color labeling: blue, Co; gray, C in GDY; green, C in intermediates and CO_2; purple, Br; red, O; and pink, H. (b) Projected density of state (PDOS) of Co-3d in Co^0/GDY (black line) and SO adsorbed Co^0/GDY (red line), respectively. (c) Differential charge density map of SO adsorbed Co^0/GDY. Yellow area represents the charge accumulation and blue area represents the charge deletion, respectively. Isosurface is set to 0.001 e/bohr^3.

bromide (TBAB, Figure S4). The variable temperature experiments were carried out in the range from 20 to 80 °C under a fixed reaction time of 10 h. GDY displays a smaller SO conversion of 19.2% than Co^0/GDY ACs at room temperature (Figures S5). With the increase of the temperatures, the SO conversion for Co^0/GDY increased significantly from 27.62% at 20 °C to nearly 100% at 80 °C (Figure 4d). The reaction selectivity kept above 99% for all reaction processes. All independent experiments (Figures 4e and S5−S17) showed a similar high SO conversion and no byproducts formed during the cycloaddition reactions, solidly demonstrating the high reaction performance and reproducibility of Co^0/GDY. As shown in Figures S18−S22 and Table S1, the catalytic performances of Co^0/GDY varied with the change of the amount of Co atoms. It was observed that all samples show the high reaction selectivity near 100% and no byproducts could be detected by NMR analysis (Figures S18−S22). The sample with the smallest mass loading showed the lowest reaction conversion of 29.33 ± 3.4%. With the increase of the concentration of Co, the conversion initially increased and reached a maximum value of 98.02 ± 2.5% and then decreased with a further *increase* of the Co contents in the samples (Figure S18−S22, Table S1).

As shown in Figure 5a, at the same reaction time, the reaction rate increases with increasing temperature; the SO conversion for Co^0/GDY at different reaction temperatures kept increasing with the increase of the reaction times. The turnover frequency (TOF) was further calculated to quantify the specific activity of the catalysts. As expected, Co^0/GDY presents the highest TOF values of 3024.8 h^{-1} (Figures 5b), which is significantly larger than those of previously reported benchmarked catalysts (Figure 5c and Table S3), and shows the highest yield (Figure 5d). Compared with the conventional metal-based catalysts, Co^0/GDY showed a great advantage in the cycloaddition of styrene oxide and CO_2 (Tables S2 and S3). More importantly, Co^0/GDY can immediately be recovered from the reaction mixture through a simply washing by ethyl acetate for the next catalytic cycle. Remarkably, the catalytic performance of Co^0/GDY could be maintained for 15 runs (Figure 5e), indicating the high stability of the as-prepared ACs. Very interestingly, Co^0/GDY also showed excellent reaction performance regarding different reactants with the high SO conversion (Figure 5f), for example, epichlorohydrin (99.99%), 1,2-epoxyhexane (98.04%), cyclohexene oxide (96.15%), glycidyl isopropyl ether (99.99%), and glycidyl phenyl ether (98.0%).

DFT Calculations

To better understand the reaction mechanisms for catalyzing the cycloaddition of styrene oxide (SO) and CO_2, density-functional theory (DFT) calculations were performed by using Co^0/GDY as the model catalyst (Figure S23a).[50,51] As shown in Figure 6a, the adsorption of SO on Co^0/GDY (intermediate II) is thermodynamically favorable with a much larger decrease in Gibbs free energy relative to the initial state I, which mainly arises from the strong bonding effect and charge transfer between the oxygen atom on SO and the Co atom on the catalyst. This is confirmed by analyzing the partial density of state (PDOS) and the differential charge density distribution (Figures S23b and 6b). As shown in Figure 6b, the PDOS of Co-3d in SO adsorbed Co^0/GDY is obviously decreased and is far away from Fermi level compared to that in Co^0/GDY,

https://doi.org/10.1021/acsmaterialsau.1c00012
ACS Mater. Au 2021, 1, 107−115

indicating the electron loss in the Co-3d orbital. The differential charge density map (Figures 6c and S24) also clearly reveals the electron loss in the Co atom and the electron gain in the O atom on SO. According to the Bader charge analysis, the deleted electron is −0.63 e in the Co atom and the gained electron is +0.88 e in the O atom, respectively. The charge transfer from atomic level Co site to SO reactant favors the subsequent activation process for the ring-opening reaction of epoxide, which is significantly exothermic. These results also indicated that the outstanding catalytic performances are mainly originated from the rapid charge transfer behavior of Co^0/GDY. After the ring-opening (intermediate III), the insertion of the CO_2 molecule (intermediate IV 3 and V) and the formation of styrene carbonate (SC, intermediate VI) through the ring-closing reaction are uphill in Gibbs free energy. However, the barriers for the two processes are very low, which are only 0.03, 0.49, and 0.15 eV, respectively. Finally, the desorption of the final product is energetically exothermic without a barrier, which can facilitate the accomplishment of the whole catalytic process.

CONCLUSIONS

In conclusion, GDY-based zerovalent Co^0/GDY ACs were found and developed via a facile preadsorption-reduction strategy. The structure of the catalysts was accurately and clearly characterized. Benefitting from the special chemical/electronic structures, Co^0/GDY show superior catalytic activities and selectivity for the cycloaddition of CO_2 and epoxide into cyclic carbonate (conversion: near 100%; selectivity > 99%), such catalysts that chemists expect. Moreover, it possesses the largest TOF value of 3024.8 h^{-1}, which is almost 30 times higher than those of benchmarked catalysts. We believe that the catalysts we have discovered will soon attract widespread attention and become the next generation of catalysts that scientists expect.

METHODS

Synthesis of 3D GDY Nanosheets Array Electrode

3D GDY nanosheet array electrodes were prepared through a simple solvothermal method. Typically, 30 mL of pyridine solution containing 10 mg of HEB was added into a Teflon-lined stainless-steel autoclave containing two piece of Cu foil and carbon cloth (CC). After a 12 h reaction at 110 °C, the GDY nanosheet grown on CC was collected and washed with HCl (3 M), hot DMF, acetone, and deionized water. Finally, the cleaned GDY was dried for at least 12 h in the vacuum oven at room temperature.

Synthesis of Co^0/GDY ACs

The zerovalent Co^0/GDY ACs were synthesized through a simple chronopotentiometry method by using a standard three-electrode system, in which the as-prepared catalysts, carbon rod, and saturated calomel electrode were used as the working electrode, counter electrode, and reference electrode, respectively. Typically, the electrochemical reduction process was carried out at the constant current density of 10 mA cm^{-2} for different times, such as 50, 100, 200, 300, and 400 s. Samples with different concentrations of Co were obtained by simply changing the electrochemical reduction time. The optimal catalyst with the best catalytic performances was obtained at the constant current density of 10 mA cm^{-2} for 200 s. The resulting Co^0/GDY was carefully washed with 0.5 M H_2SO_4, DI_{H_2O}, and acetone several times, dried in a vacuum oven at room temperature for 1 h, and then used for catalytic reaction immediately.

Cycloaddition Reactions

In a typical procedure, Co^0/GDY, tetrabutylammonium bromide (TBAB, 319 mg, 0.99 mmol), and styrene oxide (19.8 mmol) were added to a reactor under CO_2 atmosphere and at ambient pressure for different reaction times and different temperatures. The resulted mixture was analyzed by ^{1}H NMR in order to obtain the information on the yield and purity of final products.

Characterizations

The morphology of the sample was characterized by SEM (ZEISS SUPRA 55, Germany), TEM (JEM-2100F), and HR-TEM. Energy-dispersive X-ray spectroscopy (EDX) was conducted with an energy-dispersive X-ray detector in the ZEISS SUPRA 55 SEM system. HAADF-STEM images were obtained by using an aberration-corrected cubed FET Titan Cubed Themis G2 300 or JEM-ARM200F system (JEOL, Tokyo, Japan). The metal content was determined by inductively coupled plasma optical emission spectrometry (ICP-OES, Agilent ICPOES730). Raman spectra were measured through the LabRAM HR800 spectrometer (473 nm excitation laser source). XPS measurements were carried through a Thermo Scientific ESCALab 250Xi instrument with monochromatic Al Kα X-ray radiation. Nuclear magnetic resonance spectroscopy (^{1}H NMR, AVANCE III HD 400) was used to determine the yield and purity of the final products.

XAS Measurements

The acquired EXAFS data was processed according to the standard procedures using the ATHENA module implemented in the IFEFFIT software package. The k^3-weighted EXAFS spectra were obtained by subtracting the postedge background from the overall absorption and then normalizing with respect to the edge-jump step. Subsequently, k^3-weighted $\chi(k)$ data of the Co K-edge were Fourier transformed to real (R) space using a hanning window (dk = 1.0 Å^{-1}) to separate the EXAFS contributions from different coordination shells. To obtain the quantitative structural parameters around central atoms, least-squares curve parameter fitting was performed using the ARTEMIS module of the IFEFFIT software package.

ASSOCIATED CONTENT

Supporting Information

The Supporting Information is available free of charge at https://pubs.acs.org/doi/10.1021/acsmaterialsau.1c00012.

SEM, element mapping images of 3D GDY nanosheet, XPS spectra and Raman spectra of the samples, ^{1}H NMR spectra of the reaction products obtained at different reaction conditions, differential charge density maps and PDOS for the catalysts, the conversion and selectivity data for Co^0/GDY, comparison of the catalytic performances of Co^0/GDY with reported catalysts (PDF)

AUTHOR INFORMATION

Corresponding Authors

Yurui Xue − *Science Center for Material Creation and Energy Conversion, School of Chemistry and Chemical Engineering, Institute of Frontier and Interdisciplinary Science, Shandong University, Jinan 250100, P.R. China*; Email: yrxue@sdu.edu.cn

Feng He − *CAS Key Laboratory of Organic Solids, Beijing National laboratory for Molecular Sciences (BNLMS), CAS Research/Education Center for Excellence in Molecular Science, Institute of Chemistry, Chinese Academy of Sciences, Beijing 100190, P.R. China*; orcid.org/0000-0003-4820-7978; Email: hefeng2018@iccas.ac.cn

Yuliang Li − *Science Center for Material Creation and Energy Conversion, School of Chemistry and Chemical Engineering,*

https://doi.org/10.1021/acsmaterialsau.1c00012
ACS Mater. Au 2021, 1, 107−115

Institute of Frontier and Interdisciplinary Science, Shandong University, Jinan 250100, P.R. China; CAS Key Laboratory of Organic Solids, Beijing National laboratory for Molecular Sciences (BNLMS), CAS Research/Education Center for Excellence in Molecular Science, Institute of Chemistry, Chinese Academy of Sciences, Beijing 100190, P.R. China; University of Chinese Academy of Sciences, Beijing 100049, P.R. China; orcid.org/0000-0001-5279-0399; Email: ylli@iccas.ac.cn

Authors

Zhiqiang Zheng − *Science Center for Material Creation and Energy Conversion, School of Chemistry and Chemical Engineering, Institute of Frontier and Interdisciplinary Science, Shandong University, Jinan 250100, P.R. China*

Zhongqiang Wang − *Science Center for Material Creation and Energy Conversion, School of Chemistry and Chemical Engineering, Institute of Frontier and Interdisciplinary Science, Shandong University, Jinan 250100, P.R. China*

Complete contact information is available at: https://pubs.acs.org/10.1021/acsmaterialsau.1c00012

Author Contributions

Y.L. conceived and designed the research, and critically revised the manuscript. Y.X. and Y.L. supervised the project. Z.Z. performed all experiments, analyzed the data and wrote the draft. Z.W. contributed to the synthesis of GDY. Y.X. helped in analyzing data and revising the paper. F.H. conducted the theoretical calculations.

Funding

This work was supported by the National Nature Science Foundation of China (21790050, 21790051, and 22005310), the National Key Research and Development Project of China (2016YFA0200104 and 2018YFA0703501), the Key Program of the Chinese Academy of Sciences (QYZDY-SSW-SLH015), the Young Scholarship Funding of Shandong University, the Taishan Scholars Youth Expert Program of Shandong Province (tsqn201909050), and the Natural Science Foundation of Shandong Province (ZR2020ZD38).

Notes

The authors declare no competing financial interest.

■ ACKNOWLEDGMENTS

We would like to thank Professor Jun Luo at Tianjin University of Technology for his assistance in the HAADF imaging measurements. We also thank Professor Lirong Zheng at the XAFS station (beamline 1W1B) of the Beijing Synchrotron Radiation Facility.

■ REFERENCES

(1) Gattuso, J. P.; Magnan, A.; Billé, R.; Cheung, W. W. L.; Howes, E. L.; Joos, F.; Allemand, D.; Bopp, L.; Cooley, S. R.; Eakin, C. M.; Hoegh-Guldberg, O.; Kelly, R. P.; Pörtner, H. O.; Rogers, A. D.; Baxter, J. M.; Laffoley, D.; Osborn, D.; Rankovic, A.; Rochette, J.; Sumaila, U. R.; Treyer, S.; Turley, C. Contrasting futures for ocean and society from different anthropogenic CO_2 emissions scenarios. *Science* **2015**, *349*, No. aac4722.

(2) Cózar, A.; Echevarría, F.; González-Gordillo, J. I.; Irigoien, X.; Úbeda, B.; Hernández-León, S.; Palma, Á. T.; Navarro, S.; García-De-Lomas, J.; Ruiz, A.; Fernández-de-Puelles, M. L.; Duarte, C. M. Plastic debris in the open ocean. *Proc. Natl. Acad. Sci. U. S. A.* **2014**, *111*, 10239.

(3) MacDowell, N.; Florin, N.; Buchard, A.; Hallett, J.; Galindo, A.; Jackson, G.; Adjiman, C. S.; Williams, C. K.; Shah, N.; Fennell, P. An overview of CO_2 capture technologies. *Energy Environ. Sci.* **2010**, *3*, 1645−1669.

(4) Wang, Q.; Luo, J.; Zhong, Z.; Borgna, A. CO_2 capture by solid adsorbents and their applications: current status and new trends. *Energy Environ. Sci.* **2011**, *4*, 42−55.

(5) Liu, J.; Thallapally, P. K.; McGrail, B. P.; Brown, D. R.; Liu, J. Progress in adsorption-based CO_2 capture by metal-organic frameworks. *Chem. Soc. Rev.* **2012**, *41*, 2308−2322.

(6) Sumida, K.; Rogow, D. L.; Mason, J. A.; McDonald, T. M.; Bloch, E. D.; Herm, Z. R.; Bae, T.-H.; Long, J. R. Carbon dioxide capture in metal-organic frameworks. *Chem. Rev.* **2012**, *112*, 724−781.

(7) Li, J.-R.; Ma, Y.; McCarthy, M. C.; Sculley, J.; Yu, J.; Jeong, H.-K.; Balbuena, P. B.; Zhou, H.-C. Carbon dioxide capture-related gas adsorption and separation in metal-organic frameworks. *Coord. Chem. Rev.* **2011**, *255*, 1791−1823.

(8) Cokoja, M.; Bruckmeier, C.; Rieger, B.; Herrmann, W. A.; Kühn, F. E. Transformation of carbon dioxide with homogeneous transition-metal catalysts: a molecular solution to a global challenge? *Angew. Chem., Int. Ed.* **2011**, *50*, 8510−8537.

(9) Wang, W.; Wang, S.; Ma, X.; Gong, J. Recent advances in catalytic hydrogenation of carbon dioxide. *Chem. Soc. Rev.* **2011**, *40*, 3703−3727.

(10) Omae, I. Recent developments in carbon dioxide utilization for the production of organic chemicals. *Coord. Chem. Rev.* **2012**, *256*, 1384−1405.

(11) Qiao, J.; Liu, Y.; Hong, F.; Zhang, J. A review of catalysts for the electroreduction of carbon dioxide to produce low-carbon fuels. *Chem. Soc. Rev.* **2014**, *43*, 631−675.

(12) Xu, H.-Q.; Hu, J.; Wang, D.; Li, Z.; Zhang, Q.; Luo, Y.; Yu, S.-H.; Jiang, H.-L. Visible-light photoreduction of CO_2 in a metal-organic framework: boosting electron-hole separation via electron trap states. *J. Am. Chem. Soc.* **2015**, *137*, 13440−13443.

(13) Trickett, C. A.; Helal, A.; Al-Maythalony, B. A.; Yamani, Z. H.; Cordova, K. E.; Yaghi, O. M. The chemistry of metal-organic frameworks for CO_2 capture, regeneration and conversion. *Nat. Rev. Mater.* **2017**, *2*, 17045.

(14) Xue, Y.; Hui, L.; Yu, H.; Liu, Y.; Fang, Y.; Huang, B.; Zhao, Y.; Li, Z.; Li, Y. Rationally engineered active sites for efficient and durable hydrogen generation. *Nat. Commun.* **2019**, *10*, 2281.

(15) Decortes, A.; Castilla, A. M.; Kleij, A. W. Salen-Complex-mediated formation of cyclic carbonates by cycloaddition of CO_2 to epoxides. *Angew. Chem., Int. Ed.* **2010**, *49*, 9822−9837.

(16) Xu, B.-H.; Wang, J.-Q.; Sun, J.; Huang, Y.; Zhang, J.-P.; Zhang, X.-P.; Zhang, S.-J. Fixation of CO_2 into cyclic carbonates catalyzed by ionic liquids: a multi-scale approach. *Green Chem.* **2015**, *17*, 108−122.

(17) Maeda, C.; Taniguchi, T.; Ogawa, K.; Ema, T. Bifunctional catalysts based on m-phenylene-bridged porphyrin dimer and trimer platforms: synthesis of cyclic carbonates from carbon dioxide and epoxides. *Angew. Chem., Int. Ed.* **2015**, *54*, 134−138.

(18) He, H.; Perman, J. A.; Zhu, G.; Ma, S. Metal-organic frameworks for CO_2 chemical transformations. *Small* **2016**, *12*, 6309−6324.

(19) Miralda, C. M.; Macias, E. E.; Zhu, M.; Ratnasamy, P.; Carreon, M. A. Zeolitic imidazole framework-8 catalysts in the conversion of CO2 to chloropropene carbonate. *ACS Catal.* **2012**, *2*, 180−183.

(20) Beyzavi, M. H.; Klet, R. C.; Tussupbayev, S.; Borycz, J.; Vermeulen, N. A.; Cramer, C. J.; Stoddart, J. F.; Hupp, J. T.; Farha, O. K. A hafnium-based metal-organic framework as an efficient and multifunctional catalyst for facile CO_2 fixation and regioselective and enantioretentive epoxide activation. *J. Am. Chem. Soc.* **2014**, *136*, 15861−15864.

(21) Ji, G.; Yang, Z.; Zhang, H.; Zhao, Y.; Yu, B.; Ma, Z.; Liu, Z. Hierarchically mesoporous o-hydroxyazobenzene polymers: synthesis and their applications in CO_2 capture and conversion. *Angew. Chem., Int. Ed.* **2016**, *55*, 9685−9689.

(22) Liu, D.; Li, G.; Liu, J.; Wei, Y.; Guo, H. Mesoporous titanium-silicalite zeolite containing organic templates as a bifunctional catalyst

for cycloaddition of CO_2 and epoxides. *ACS Appl. Mater. Interfaces* **2018**, *10*, 22119−22129.
(23) Feng, D.; Chung, W.-C.; Wei, Z.; Gu, Z.-Y.; Jiang, H.-L.; Chen, Y.-P.; Darensbourg, D. J.; Zhou, H.-C. Construction of ultrastable Porphyrin Zr metal-organic frameworks through linker elimination. *J. Am. Chem. Soc.* **2013**, *135*, 17105−17110.
(24) Liang, L.; Liu, C.; Jiang, F.; Chen, Q.; Zhang, L.; Xue, H.; Jiang, H.-L.; Qian, J.; Yuan, D.; Hong, M. Carbon dioxide capture and conversion by an acid-base resistant metal-organic framework. *Nat. Commun.* **2017**, *8*, 1233.
(25) Yang, Q.; Yang, C.-C.; Lin, C.-H.; Jiang, H.-L. Metal-organic-framework-derived hollow N-doped porous carbon with ultrahigh concentrations of single Zn atoms for efficient carbon dioxide conversion. *Angew. Chem., Int. Ed.* **2019**, *58*, 3511−3515.
(26) Qiao, B.; Wang, A.; Yang, X.; Allard, L. F.; Jiang, Z.; Cui, Y.; Liu, J.; Li, J.; Zhang, T. Single-atom catalysis of CO oxidation using $Pt1/FeO_x$. *Nat. Chem.* **2011**, *3*, 634−641.
(27) Liu, P.; Zhao, Y.; Qin, R.; Mo, S.; Chen, G.; Gu, L.; Chevrier, D. M.; Zhang, P.; Guo, Q.; Zang, D.; Wu, B.; Fu, G.; Zheng, N. Photochemical route for synthesizing atomically dispersed palladium catalysts. *Science* **2016**, *352*, 797.
(28) Jones, J.; Xiong, H.; DeLaRiva, A. T.; Peterson, E. J.; Pham, H.; Challa, S. R.; Qi, G.; Oh, S.; Wiebenga, M. H.; Pereira Hernández, X. I.; Wang, Y.; Datye, A. K. Thermally stable single-atom platinum-on-ceria catalysts via atom trapping. *Science* **2016**, *353*, 150.
(29) Hui, L.; Xue, Y.; Yu, H.; Liu, Y.; Fang, Y.; Xing, C.; Huang, B.; Li, Y. Highly efficient and selective generation of ammonia and hydrogen on a graphdiyne-based catalyst. *J. Am. Chem. Soc.* **2019**, *141*, 10677−10683.
(30) Xue, Y.; Huang, B.; Yi, Y.; Guo, Y.; Zuo, Z.; Li, Y.; Jia, Z.; Liu, H.; Li, Y. Anchoring zero valence single atoms of nickel and iron on graphdiyne for hydrogen evolution. *Nat. Commun.* **2018**, *9*, 1460.
(31) Sun, M.; Wu, T.; Dougherty, A. W.; Lam, M.; Huang, B.; Li, Y.; Yan, C.-H. Self-validated machine learning study of graphdiyne-based dual atomic catalyst. *Adv. Energy Mater.* **2021**, *11*, 2003796.
(32) Sun, M.; Wu, T.; Xue, Y.; Dougherty, A. W.; Huang, B.; Li, Y.; Yan, C.-H. Mapping of atomic catalyst on graphdiyne. *Nano Energy* **2019**, *62*, 754−763.
(33) Zuo, Z.; Li, Y. Emerging Electrochemical Energy Applications of Graphdiyne. *Joule* **2019**, *3*, 899−903.
(34) Gao, X.; Liu, H.; Wang, D.; Zhang, J. Graphdiyne: synthesis, properties, and applications. *Chem. Soc. Rev.* **2019**, *48*, 908−936.
(35) Huang, C.; Li, Y.; Wang, N.; Xue, Y.; Zuo, Z.; Liu, H.; Li, Y. Progress in research into 2D graphdiyne-based materials. *Chem. Rev.* **2018**, *118*, 7744−7803.
(36) Hui, L.; Xue, Y.; Yu, H.; Zhang, C.; Huang, B.; Li, Y. Loading copper atoms on graphdiyne for highly efficient hydrogen production. *ChemPhysChem* **2020**, *21*, 2145−2149.
(37) Xue, Y.; Huang, B.; Yi, Y.; Guo, Y.; Zuo, Z.; Li, Y.; Jia, Z.; Liu, H.; Li, Y. Anchoring zero valence single atoms of nickel and iron on graphdiyne for hydrogen evolution. *Nat. Commun.* **2018**, *9*, 1460.
(38) Yu, H.; Xue, Y.; Hui, L.; Zhang, C.; Fang, Y.; Liu, Y.; Chen, X.; Zhang, D.; Huang, B.; Li, Y. Graphdiyne based metal atomic catalysts for synthesizing ammonia. *Nat. Sci. Rev.* **2020**, nwaa213.
(39) Zhang, S.; Si, H.; Fan, W.; Shi, M.; Li, M.; Xu, C.; Zhang, Z.; Liao, Q.; Sattar, A.; Kang, Z.; Zhang, Y. Graphdiyne: bridging SnO_2 and perovskite in planar solar cells. *Angew. Chem., Int. Ed.* **2020**, *59*, 11573−11582.
(40) Xue, Y.; Li, Y.; Zhang, J.; Liu, Z.; Zhao, Y. 2D graphdiyne materials: challenges and opportunities in energy field. *Sci. China: Chem.* **2018**, *61*, 765−786.
(41) Fang, Y.; Xue, Y.; Hui, L.; Yu, H.; Li, Y. Graphdiyne@Janus magnetite for photocatalytic nitrogen fixation. *Angew. Chem., Int. Ed.* **2021**, *60*, 3170−3174.
(42) Xing, C.; Xue, Y.; Huang, B.; Yu, H.; Hui, L.; Fang, Y.; Liu, Y.; Zhao, Y.; Li, Z.; Li, Y. Fluorographdiyne: a metal-free catalyst for applications in water reduction and oxidation. *Angew. Chem., Int. Ed.* **2019**, *58*, 13897−13903.
(43) Yu, H.; Xue, Y.; Li, Y. Graphdiyne and its assembly architectures: synthesis, functionalization, and applications. *Adv. Mater.* **2019**, *31*, 1803101.
(44) Hui, L.; Xue, Y.; Jia, D.; Yu, H.; Zhang, C.; Li, Y. Multifunctional single-crystallized carbonate hydroxides as highly efficient electrocatalyst for full water splitting. *Adv. Energy Mater.* **2018**, *8*, 1800175.
(45) Wang, F.; Zuo, Z.; Li, L.; Li, K.; He, F.; Jiang, Z.; Li, Y. Large-area aminated-graphdiyne thin films for direct methanol fuel cells. *Angew. Chem., Int. Ed.* **2019**, *58*, 15010−15015.
(46) Shang, H.; Zuo, Z.; Li, L.; Wang, F.; Liu, H.; Li, Y.; Li, Y. Ultrathin graphdiyne nanosheets grown in situ on copper nanowires and their performance as lithium-ion battery anodes. *Angew. Chem., Int. Ed.* **2018**, *57*, 774−778.
(47) Wang, N.; Li, X.; Tu, Z.; Zhao, F.; He, J.; Guan, Z.; Huang, C.; Yi, Y.; Li, Y. Synthesis and electronic structure of boron-graphdiyne with an sp-hybridized carbon skeleton and its application in sodium storage. *Angew. Chem., Int. Ed.* **2018**, *57*, 3968−3973.
(48) He, J.; Ma, S.; Zhou, P.; Zhang, C. X.; He, C.; Sun, L. Z. Magnetic properties of single transition-metal atom absorbed graphdiyne and graphyne sheet from DFT+U calculations. *J. Phys. Chem. C* **2012**, *116*, 26313−26321.
(49) Zhang, Z.; Feng, C.; Liu, C.; Zuo, M.; Qin, L.; Yan, X.; Xing, Y.; Li, H.; Si, R.; Zhou, S.; Zeng, J. Electrochemical deposition as a universal route for fabricating single-atom catalysts. *Nat. Commun.* **2020**, *11*, 1215.
(50) Xin, X.; Shan, H.; Tian, T.; Wang, Y.; Yuan, D.; You, H.; Yao, Y. Conversion of CO_2 into cyclic carbonates under ambient conditions catalyzed by rare-earth metal complexes bearing poly-(phenolato) ligand. *ACS Sustainable Chem. Eng.* **2020**, *8*, 13185−13194.
(51) Yang, G.-W.; Zhang, Y.-Y.; Xie, R.; Wu, G.-P. Scalable bifunctional organoboron catalysts for copolymerization of CO_2 and epoxides with unprecedented efficiency. *J. Am. Chem. Soc.* **2020**, *142*, 12245−12255.

https://doi.org/10.1021/acsmaterialsau.1c00012
ACS Mater. Au 2021, 1, 107−115